SLENDER FOREBODY AERODYNAMICS AT HIGH ALPHA

K.Petterson & D.I.A.Poll
College of Aeronautics,
Cranfield University,
Bedfordshire,
MK43 0AL,
United Kingdom

Keywords: *CFD, Forebody, High Angle-of-Attack, Vortex Asymmetry*

Abstract

Combat aircraft forebody vortex flow at high angles of attack is complex and non-linear: the stable and symmetric vortices generated by the nose at lower angles can become asymmetric and unstable as alpha is increased. The forces and moments resulting from such asymmetry may be the determining factor for control power and thus it is necessary to be able to predict the high-alpha characteristics of the forebody accurately as early as possible in the design process. CFD should be the ideal evaluation tool, however, this problem has been shown numerous times to be a challenge for computational simulation.

Using the NSMB Navier-Stokes Multi-Block code, an attempt is being made to develop an improved, more physically representative, approach to dealing with this type of problem. Results from preliminary computations using tip excrescences and non-symmetrical solution methods on a tangent-ogive geometry are presented, together with initial solutions for the Saab JAS-39 Gripen forebody.

The next stages in the work and proposed code improvements for tackling high angle-of-attack forebody flows are also briefly discussed.

Nomenclature

C_d	drag coefficient
C_l	lift coefficient
C_p	pressure coefficient
C_y	sideforce coefficient
D	base diameter
M	Mach number
Re	Reynolds number
T	temperature
U	velocity
a	speed of sound
p	pressure
ρ	density
∞	denotes freestream value

1 Introduction

Recent years have seen combat aircraft become increasingly agile. Subsonic manoeuvers such as the Herbst manoeuver or the Cobra were unthinkable a few years ago, but the modern dogfighter *has* to be capable of operating effectively throughout the high-alpha regime. It is well known that a key factor affecting the stability and control of the aircraft in these conditions is the behaviour of the vortex flowfield generated in the lee of the forebody. Large sideforces and yawing moments can be generated by the nose vortices, even at zero sideslip, whilst conventional control power may be limited by blanking of the tail and rudder by the fuselage. In extreme cases this may lead to directional instability and spin departure.

Manipulation and control of the nose vortices to stabilise the aircraft is an obvious solution. A number of systems have been proposed including boundary-layer devices, passive and active strakes and slot or port blowing/suction.

Partly funded by Saab Aerospace, this ongoing research has the objective of developing an improved computational approach for high-alpha forebody flow using the CFD code *NSMB*. The difficulties associated with the computational prediction of such flows have been well documented over the past ten years or so, (see for example [3, 6, 9]), and mainly stem from uncertainty over the exact mechanisms driving the flowfield. Even for simplified tangent-ogive forebodies, wind-tunnel tests have shown the magnitude and direction of the sideforces to be sensitive to Mach number, roll angle, free-stream turbulence level, surface roughness and microscopic tip asymmetries. The Reynolds numbers typical of subsonic manoeuvering flight are also low enough to result in large regions of laminar or transitional flow remaining near the nose apex, as was evident during flight test of the NASA F-18 HARV[1]. Clearly then, as with the numerical modelling of any physical system, certain simplifying assumptions must be made. However, the nature of the forebody vortex problem is such that if subtleties are ignored totally the resulting model may be so far removed from reality that the results are meaningless.

The nature of the vortex wake changes considerably as the angle of attack of the forebody increases, but can be described as moving through four main phases: stable symmetric vortices; stable asymmetric vortices; unstable asymmetric vortices; time dependent Karmann shedding. The initial aim of the project was to produce a modelling methodology that would enable the flowfield around an arbitrary slender forebody to be computed at any angle of attack. However, it was quickly realised that this is no trivial task. The area of interest has thus been narrowed to the first and second phases in the development of the flow.

[1]High Alpha Research Vehicle

2 Computational Details

2.1 The Numerical Solver

The flow solver being used for this work is *NSMB*, [13], a three-dimensional multiblock Navier-Stokes code being developed as a joint research project by two universities, (EPFL in Lausanne, Switzerland, and KTH in Stockholm, Sweden), a research institute, (CERFACS, Toulouse, France), and two industrial partners, (Aerospatiale Avions of France and Saab Aerospace of Sweden). Several time- and space-marching schemes are implemented, solution acceleration is available through multigrid and preconditioning, and turbulent closure can be achieved utilising any one of a number of algebraic, one- or two-equation models. Aside from the computations involving tip excrescences, all computations have been run using implicit scalar LU-SGS time integration, [7], and a central spatial discretisation. Multigrid and preconditioning, although available, were not used. Turbulent closure for these initial computations was achieved with the one-equation model of Spalart-Allmaras, [11]. Domain decomposition to enable parallel computation on Cray T3E is accomplished using MB-Split, [14], a mesh partitioning tool developed at KTH.

2.2 Grids

For the initial evaluation of the existing code, the chosen geometry was the ogive-cylinder combination tested experimentally by Lamont in the NASA Ames 12ft low turbulence wind-tunnel, [8]. In Lamont's experiments, a 152.4mm (6in) diameter 3.5 calibre tangent-ogive forebody was mated to a 4.0 calibre cylindrical afterbody, giving a total model length of 1143mm. Pressure data was taken from circumferential tappings at 12 axial locations along the model for $20^o \leq \alpha \leq 90^o$, with 12 roll orientations examined at each angle of attack.

The first grid used, G3, is H-O type, with $62 \times 69 \times 78$ cells in the axial, radial and circumferential directions giving a total grid size of 333,684. Small geometric imperfections were su-

perimposed on the initial axisymmetric grid by radially displacing two surface vertices at the first station downstream of the forebody apex. Three modified grids were created with a small bump at 90^o to the windward meridian, the cell vertices being displaced by 1mm, 0.5mm and 0.1mm respectively[2].

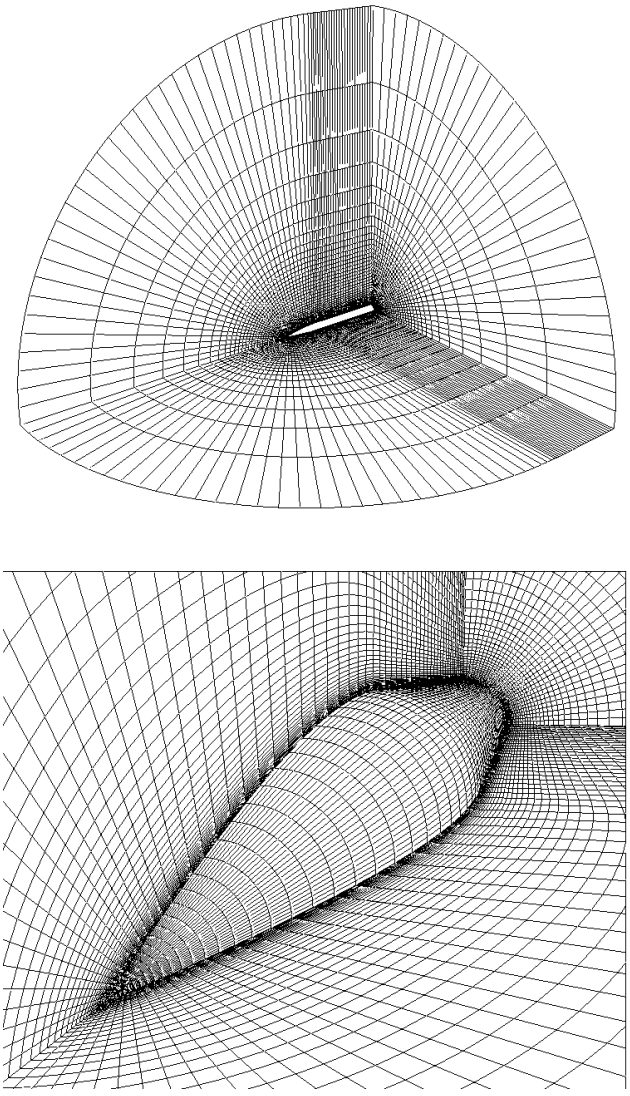

Fig. 1 : *3.5D tangent-ogive grid G5.* $60 \times 80 \times 120$ *giving* $576,000$ *cells.*

For the subsequent calculations with the non-symmetric LU-SGS algorithm, a new C-O grid was produced, G5, which addressed the deficiencies of the previous grid with respect to cell size and clustering. G5 was produced using the ICEMCFD 3-D meshing package with CAD surface mapping and is, as a result, not axisymmetric. It is, however, symmetric about the pitching plane. Grid size is $60 \times 80 \times 120$, giving a total of 576,000 cells. The cylindrical afterbody was extended by a further 3.0D, giving a total L/D of 10.5. A hemisphere-cylinder farfield boundary was generated with $R_{max}/D = 30$ at the exit plane. Two views are shown in Fig.(1).

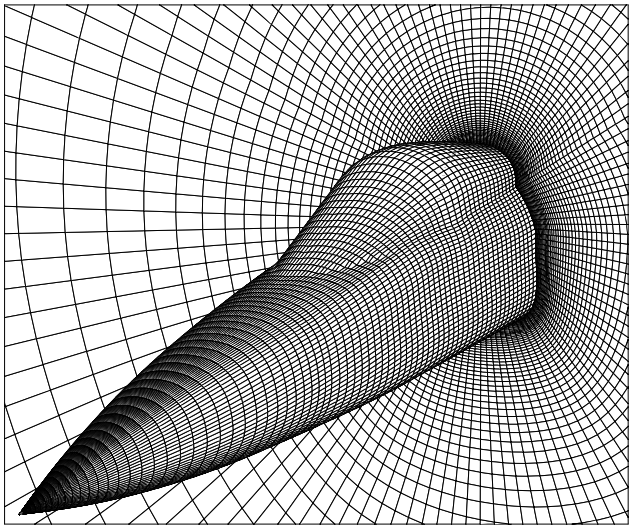

Fig. 2 : *JAS-39 grid BSL1, C-O grid,* $74 \times 85 \times 120$ *giving* $754,800$ *cells.*

Two different grids have been used for the JAS-39 computations, these being referred to as BSL1 and BSL2, where BSL denotes the baseline or 'clean' forebody without pitot-tube, nose-tip strakes or rhino-horn[3]. Both grids were of C-O type with the outer domain of the mesh forming a hemisphere-cylinder, the radius of which was 50m full-scale for grid BSL1 and 100m full-scale for grid BSL2. Grid sizes were $74 \times 85 \times 120$ and $74 \times 101 \times 120$ respectively, with BSL2 having an improved boundary-layer mesh as well as the extended farfield. The surface mesh, which was identical for both grids, is shown in Fig.(2). By far the most serious problem encountered during

[2]Corresponding to h/D=0.066, 0.0033, 0.00066

[3]Each computation has been given a run number, e.g. bsl1001 denotes run number 001 on grid bsl1.

the mesh generation process was the question of the exit boundary. For low angle-of-attack calculations it would be appropriate to extend the rearmost cross-section of the forebody prismatically. However, at high angles-of-attack this extension would generate additional vortices which would interact with those on the forebody. The answer was to simply truncate the domain at the rear of the forebody. The final boundary-conditions chosen were free-stream for the outer domain and linear extrapolation for the exit. These conditions were also used for the earlier ogive computations.

The relevant flow conditions are tabulated below in Tables (1) & (2).

	Case 1	*Case 2*
Re_D	$200,000$	$800,000$
Re/m	1.312×10^6	5.249×10^6
Mach No.	0.2	0.2
$\rho_\infty\ (kg/m^3)$	0.300	1.198
$P_\infty\ (kPa)$	24.63	98.51
$T_\infty\ (K)$	286.6	286.6
$a_\infty\ (m/s^2)$	339.346	339.346
$U_\infty\ (m/s)$	67.9	67.9

Table 1: *Flow conditions for tangent-ogive calculations (from Lamont)*

3 Preliminary Results

3.1 Tip excrescences

Tip excrescences are a well-known method of generating vortex asymmetry, see for example Degani, [1], and Degani & Levy, [2]. A computation was run at $\alpha = 40^o$ for the tangent-ogive geometry with each of three different sized excrescences. Each calculation was initialised with a converged $\alpha = 40^o$ Spalart-Allmaras solution for the unmodified configuration and the computations continued, using the same turbulence model, until the normalised density residual had dropped to below 0.1×10^{-7}, a level of convergence far greater than that required for stable force coefficients. This model, [11] was chosen for all the preliminary calculations since it has developed a reputation for being considerably more robust than two-equation models whilst also being capable of resolving complicated flowfields reasonably well.

	Case 1
Re_L	3.174×10^6
Re/m	4.059×10^6
Mach no.	0.176
$\rho_\infty\ (kg/m^3)$	1.225
$p_\infty\ (kPa)$	101.3
$T_\infty\ (K)$	288.2
$a_\infty\ (m/s^2)$	340.0
$U_\infty\ (m/s)$	60.0

Table 2: *Flow conditions for JAS-39 calculations (Saab AB)*

Comparing overall force and moment values generated by each configuration showed that the addition of a bump could increase normal force by as much as 22% above the 'clean' value, and generate a sideforce almost equal in magnitude to the normal force on the unmodified geometry. The two larger bumps produced comparable increases in normal force but that generated by the smallest bump was significantly lower. This seems to indicate that there may be a critical size for the bump when trying to provoke asymmetry in this way[4]. The computed circumferential pressure coefficient distributions for the bump calculations are compared with those obtained experimentally by Lamont in Fig.(3). It should be noted here that the experimental data was gathered at $Re_D = 0.8 \times 10^6$, whereas the computation was run under the case 1 conditions, see Tab.(1). The data is compared in this way since the computation was run fully turbulent and thus cannot be meaningfully compared with experimental data taken when large regions of laminar or transitional flow exist.

[4]It is worth noting here that only overall sideforce along the body has been considered and, generally speaking, this is not an adequate measure of the degree of asymmetry of the vortex wake. It is, of course, possible for the flow to be highly asymmetric but with the sideforce distribution giving a net value of zero. In this case, however, the asymmetry generated by the smallest bump was negligible.

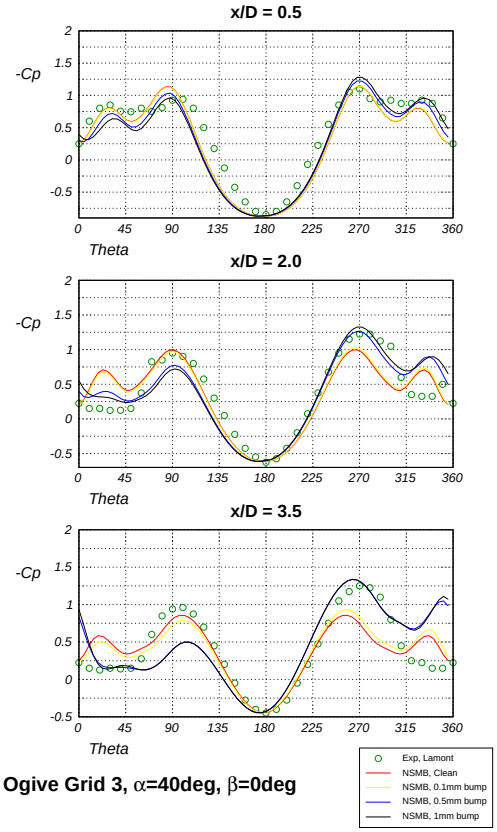

Fig. 3 : *Tangent-Ogive C_p profiles for clean configuration and with bumps, Grid G3, $\alpha = 40^o$, Case 2 conditions. All calculations run with R-K4.*

Unsurprisingly, continuation of the calculations with the bumps removed caused the flow to lapse back into symmetry.

3.2 LU-SGS Algorithm

The possibility of using an LU-SGS scheme to calculate asymmetric flow has been demonstrated by Vanden & Belk, [12], and Hwang & Rho, [6]. A small, transient, numerical error is present due to the non-symmetric factorisation of the scheme and, whilst this has negligible effect at low alpha, an asymmetric flowfield develops at high angles of attack. Hwang & Rho showed the asymmetric flowfield to be stable when the calculation was continued using a symmetric solver.

In order to ascertain whether the LU-SGS scheme in *NSMB* was capable of producing a symmetric flowfield at low angles of attack, several computations were run on G5 at $\alpha = 20^o$ under case 1 conditions. No turbulence modelling was used at first to remove one possible source of complication.

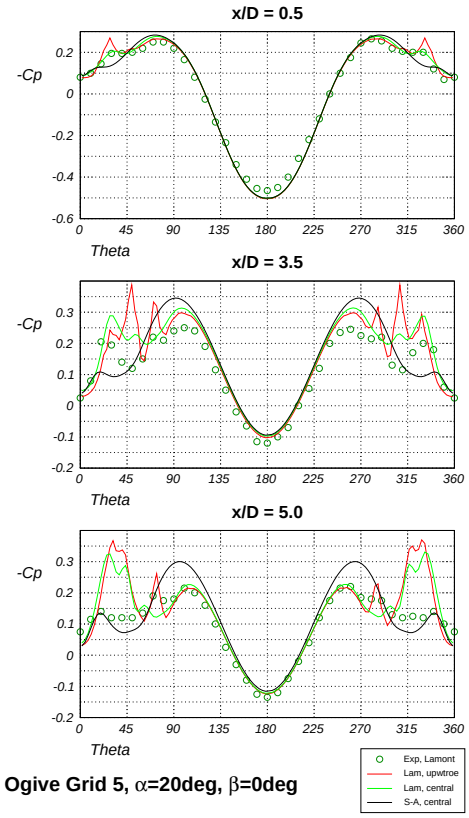

Fig. 4 : *Tangent-Ogive C_p profiles, Grid G5, $\alpha = 20^o$, Case 1 conditions. All calculations run with LU-SGS.*

Running with the upwind third-order Roe scheme, convergence effectively ceased when the normalised residual had reached approximately 1.0×10^{-4}. By this time, sideforce had almost settled at zero but was still oscillating slightly. Agreement with the C_p data of Lamont is reasonable near the nose, see Fig.(4). Further aft, however, whilst the computed C_p is accurate to approximately 90^o either side of the windward generator, $(\theta = 180^o)$, from $(\theta = 90^o)$ and $(\theta = 270^o)$ round to the leeward generator, $(\theta = 0^o)$, there are large pressure peaks and troughs. These correspond to several vortices which are not present in the real wake but seem to be

purely a result of the absence of turbulence in the computation. This appears to have been confirmed by several calculations run using the LU-SGS scheme with the central spatial discretisation. Looking again at Fig.(4), it is clear that this combination proved more suited to the problem than that used initially, even with no second-order damping and fourth-order damping set low. However, switching to the central scheme did not produce an improved flowfield prediction.

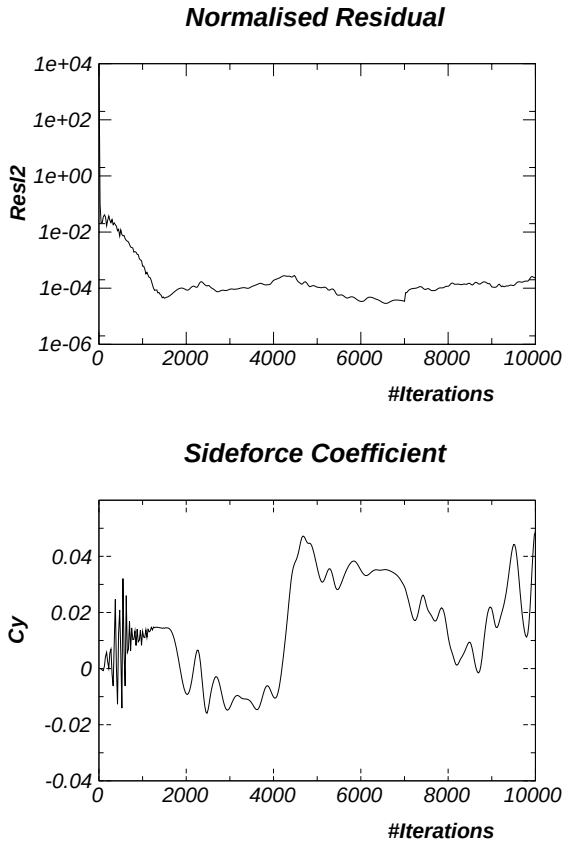

Fig. 5 : *Convergence history, tangent-ogive grid G5, laminar computation, LU-SGS,* $\alpha = 40^o$

Introducing the Spalart-Allmaras model, calculations run at $\alpha = 20^o$ and case 1 conditions converged rapidly and almost monotonically to a zero sideforce solution. The computed C_p profiles can be seen in Fig.(4). Whilst agreement near the nose is not as good as for the laminar calculations, the match with experiment is significantly improved downstream, emphasising the mixed laminar/turbulent nature of the real flowfield.

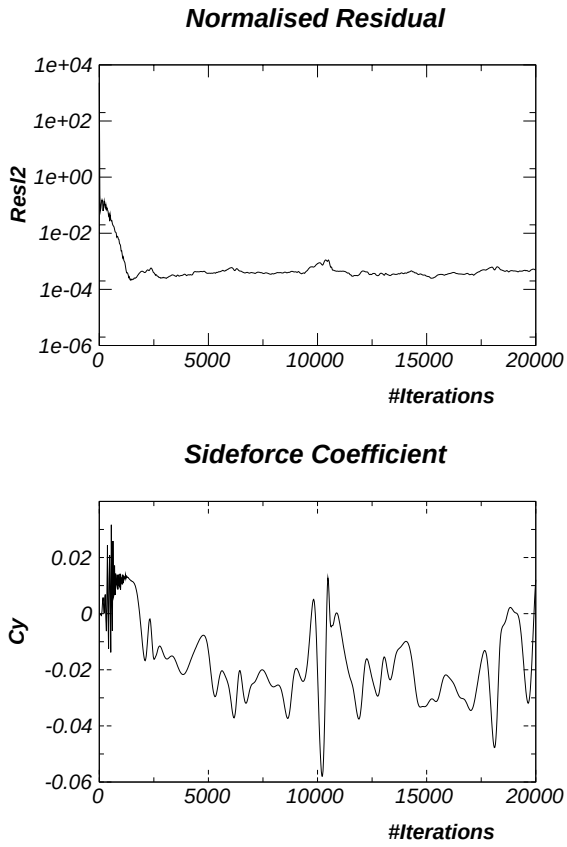

Fig. 6 : *Convergence history, tangent-ogive grid G5, turbulent computation (Spalart-Allmaras), LU-SGS,* $\alpha = 40^o$

At $\alpha = 40^o$ and case 2 conditions, where the flowfield was shown by Lamont to be highly asymmetric, no converged solution could be produced either with the purely laminar calculation or with the Spalart-Allmaras model. Time histories of normalised density residual and sideforce coefficient are shown in Figures (5) & (6). In both cases the oscillations seem almost completely random in nature with the solution not even shifting between the bistable states suggested by Fiddes, [4]. It did not prove possible to stabilise these sideforces either by increasing the artificial dissipation or, in the case of the Roe Scheme, changing limiter.

3.3 JAS-39 forebody

Solutions have been obtained at $\alpha = 0^o$, 20^o, 40^o and 50^o for both JAS-39 grids. The convergence histories for the solutions obtained at $\alpha = 0^o$ and

$\alpha = 50^o$ at zero sideslip on both grids are shown in Figures (7) & (8). Evaluating these first, a noticeable reduction in the level of convergence achieved can be seen with the 50^o solutions compared to those at lower α for grid BSL1. The residual becomes relatively oscillatory and 'bottoms out', however, the level of convergence is markedly better with the second grid. This is thought to be due to the higher cell density in the near-forebody region. (Obviously the required region of high cell density will necessarily increase in extent as α increases, since the vortices will be moving further away from the surface. All calculations were run for 5000 iterations with identical CFL numbers and other numerical parameters.

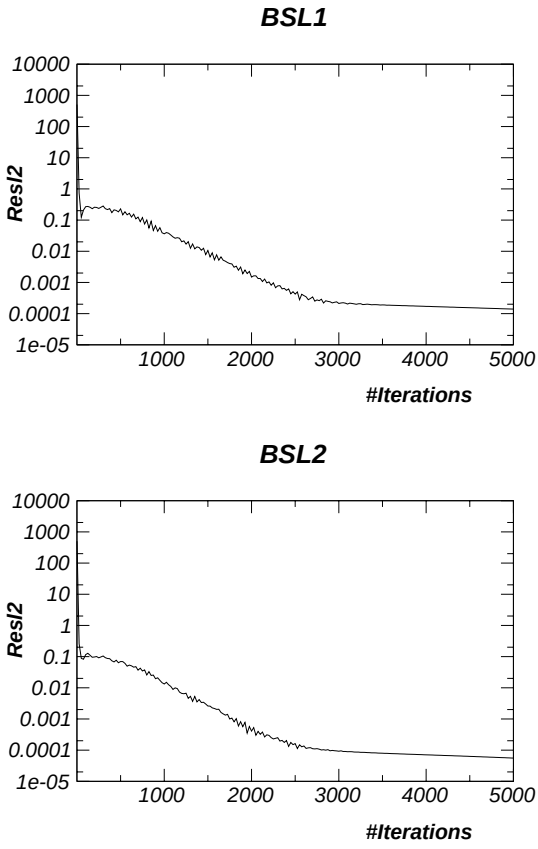

Fig. 7 : *Normalised density residuals, JAS-39 geometry,* $\alpha = 0^o$

Computed surface C_p at each longitudinal section has been plotted versus angular location around the forebody, with $\theta = 0^o$ the upper meridian and θ increasing in a clockwise direction looking aft. Fig.(9) shows experimental

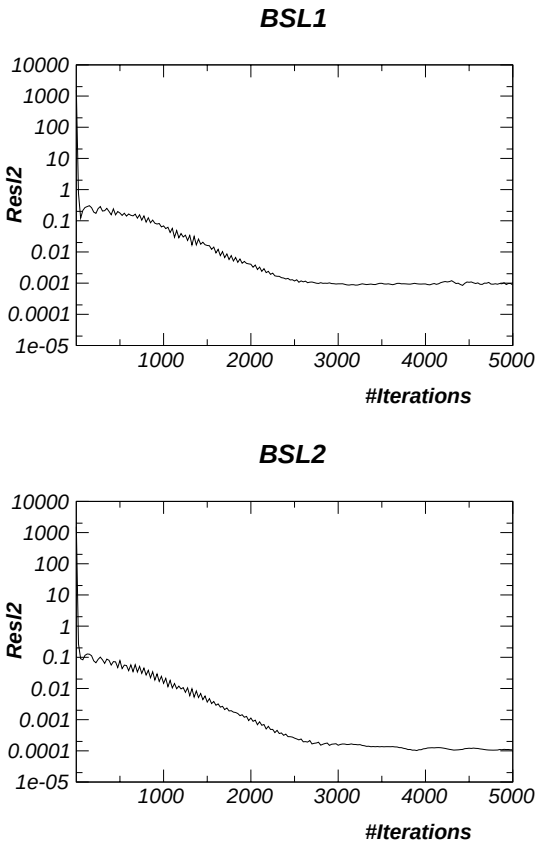

Fig. 8 : *Normalised density residuals, JAS-39 geometry,* $\alpha = 50^o$

and computed C_p at sections 1, 7 and 14 (6.2%, 26.1% and 76.2% of model length) for $\alpha = 0^o$ on BSL2. It can be seen that, as for the tangent-ogive calculations, agreement is poor where the flow is laminar or transitional near the nose but improves further aft. The position of the longitudinal vortices has been predicted correctly but vortex strength, particularly further aft is noticeably weaker than experiment shows to be the case. Increased cell densities may improve this. Agreement with experiment was improved for the $\alpha = 20^o$ computation (not shown here), although vortex strength was still low towards the rear of the body. The inability of the turbulence model to accurately resolve the vortex structure are clearly demonstrated in the C_p profiles for the $\alpha = 50^o$ calculation, see Fig.(10). Surface C_p for the $\alpha = 50^o$ computation on grid BSL1 is shown as Fig.(11(a)). Slight vortex asymmetry was computed at $\alpha = 50^o$, this being visible in the particle trace shown in Fig.(11(b)).

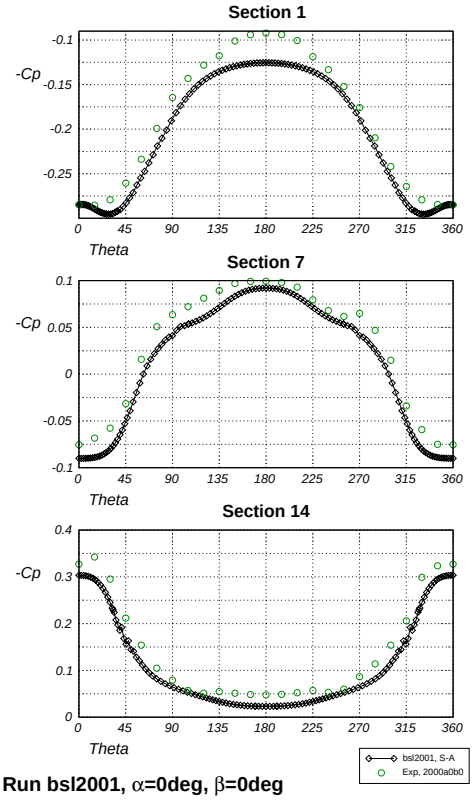

Fig. 9 : *JAS-39 C_p profiles,* $\alpha = 0^o$

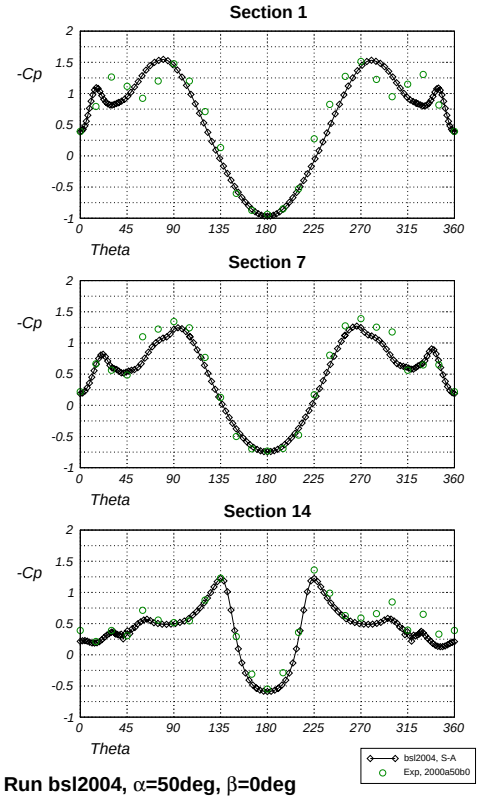

Fig. 10 : *JAS-39 C_p profiles,* $\alpha = 50^o$

4 Concluding Remarks

From the initial computational studies presented above, it has been concluded that previous approaches to dealing with high-alpha forebody flows are not physically representative enough of the problem to allow either qualitative or quantitative prediction of such flowfields.

All future work will be based around the JAS-39 Gripen forebody geometry supplied by Saab Aerospace. The baseline forebody grid shown in Fig.(2) will be expanded to include the Pitot-tube and nose strakes to mirror the production nose before a small vertical strake, known as a rhino-horn, is added near the apex. The rhino-horn acts as a splitter-plate when in a central position, preventing interaction between the nose vortices just after formation, but it can be pivoted about a vertical axis to add a measure of active control. Solutions are to be obtained using the modified code with the *k*-ω-*SST* turbulence model. The corrections proposed by Hellsten, [5], to account for streamline curvature are also be be included. It is also intended to simulate the effects of boundary-layer transition in some way, either by the imposition of a transition plane or by including a local Reynolds number based transition trigger in a low Reynolds number version of the *k*-ω-*SST* model as in the work of Liu & Tsai, [10]. Transition is an important, but often ignored, feature of forebody flow and its inclusion should significantly improve the correlation of the computational solutions with experiment.

Acknowledgements

This research is being jointly funded by the United Kingdom Engineering and Physical Sciences Research Council (EPSRC) and the Future Products and Technology Division, Saab AB. Supercomputing resources are kindly being provided by the Swedish National Supercomputer Centre, Linköping, in conjunction with the Royal Institute of Technology, Stockholm.

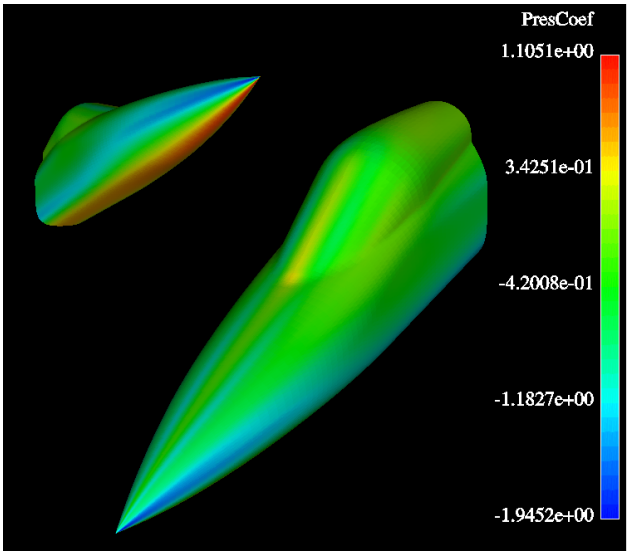

(a) Surface C_p, bsl1005, α=50^o, β=0^o

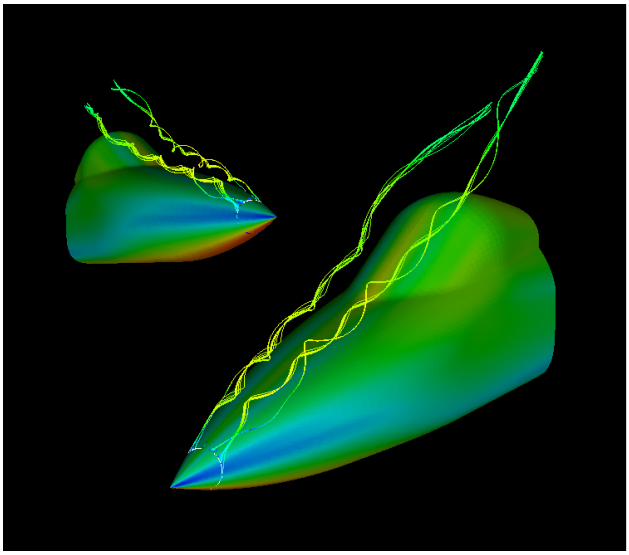

(b) Vortex Cores, bsl1005 α=50^o, β=0^o

Fig. 11 : *Surface C_p contours, JAS-39 forebody grid bsl1. Computations were fully turbulent using Spalart-Allmaras.*

References

[1] Degani D. Effect of geometric disturbance on vortex asymmetry. *AIAA Journal*, Vol. 29, No 4, pp 560–566, April 1991.

[2] Degani D and Levy Y. Asymmetric turbulent vortical flows over slender bodies. *AIAA Journal*, Vol. 30, No 9, pp 2267–2273, September 1992.

[3] Degani D, Schiff L, and Levy Y. Physical considerations governing computation of turbulent flows over bodies at large incidence. AIAA Paper 90-0096, 1990.

[4] Fiddes S. A theory of the separated flow past a slender elliptic cone at incidence. RAE Tech Memo TM1858, 1980.

[5] Hellsten A. Some improvements in Menter's *k*-ω-*sst* turbulence model. AIAA Paper 98-2554, 1998.

[6] Hwang S and Rho O. Numerical simulation of asymmetric vortical flows on a slender body at high incidence. AIAA Paper 95-1799, 1995.

[7] Jameson A and Yoon S. Lower-upper implicit schemes with multiple grids for the euler equations. *AIAA Journal*, Vol. 25, No 7, pp 929–935, July 1987.

[8] Lamont P. The complex asymmetric flow over a 3.5d ogive nose and cylindrical afterbody at high angles of attack. AIAA Paper 82-0053, 1982.

[9] Levy Y, Hesselink L, and Degani D. Systematic study of the correlation between geometrical disturbances and flow asymmetries. *AIAA Journal*, Vol. 34, No 4, pp 772–777, April 1996.

[10] Liu S and Tsai H. Simulation of boundary layer transition with a modified *k*-ω model. AIAA Paper 98-0340, 1998.

[11] Spalart P and Allmaras S. A one-equation turbulence model for aerodynamic flows. AIAA Paper 92-0439, 1992.

[12] Vanden K and Belk D. Numerical investigation of subsonic and supersonic asymmetric vortical flow. AIAA Paper 91-2869, 1991.

[13] Vos J. *et al.* NSMB 5.0 handbook. Technical Report: LMF-DGM-EPFL, CERFACS, Dept. Aeronautics KTH, Aerospatiale Matra Airbus, SAAB AB, 2000.

[14] Ytterström A. MB-Split: A structured mesh partitioning tool for load-balancing on mimd computers. in *Proceedings of the Second ECCOMAS Conference on Numerical Methods in Engineering, Paris, France*, 1996.